Proceedings of the 11th Brazilian Congress of Thermal Sciences and Engineering -- ENCIT 2006
Braz. Soc. of Mechanical Sciences and Engineering -- ABCM, Curitiba, Brazil,- Dec. 5-8, 2006

Paper CIT06-0682

INDUSTRIAL PROCESS SIMULATION BASED ON MULTIPHASE MATHEMATICAL MODEL: APPLICATION TO PREDICT THE SINTER PLANT OPERATION

José Adilson de Castro
Pós-Graduação em Engenharia Metalúrgica-EEIMVR-UFF, Av. dos Trabalhadores 420 – Vila Sta. Cecília – 27255-125 – Volta Redonda – RJ
adilson@metal.eeimvr.uff.br

Alexandre José da Silva
Pós-Graduação em Engenharia Metalúrgica-EEIMVR-UFF, Av. dos Trabalhadores 420 – Vila Sta. Cecília – 27255-125 – Volta Redonda – RJ
ajs@metal.eeimvr.uff.br

Hiroshi Nogami
IMRAM- Institute for Multidisciplinary Research for Advanced Materials-Tohoku University, 2-1-1, Katahira, Aoba-ku – Sendai. 980-8577 – Japan
nogami@tagen.tohoku.ac.jp

Jun-ichiro Yagi
Emeritus Professor of Tohoku University – Sendai, 982-0261- Japan
yagij@earth.ocn.ne.jp

Abstract: The sintering process is a well established process in use at the integrated steel industry. The process is complex involving various physical and chemical phenomena. The raw materials used can vary to a wide extent, from iron ore to dust recycling. The process takes place in a moving strand where a mixture of iron ore (sinter feed), fine coke, limestone and water is continuously charged to form a thick bed of approximately 40cm. Along the first meters of the strand the charge is ignited by burners. The hot gas, generated by the combustion of natural gas with air, is then sucked in through the packed bed from the wind boxes placed below the grate. Models to predict the operational parameters and determine optimum conditions are of great importance due to the low cost and the ability to investigate conditions which can not be assessed by experimental techniques. In this paper a mathematical model based on the multiphase multi-component transport equations is used to investigate the industrial scale operation. The transport equations are discretized based on the finite volume method and rate equations for momentum, energy and chemical reactions are used to consider the inter-phase interactions. The model predictions are in agreement with the averaged values measured at the gas outlet of the sinter strand which validated the modeling approach.

Key-words: Mathematical modeling, Sintering Plant, multi-phase, Transport phenomena

1. Introduction

The sintering process is an established process in use at the integrated route of steel production. The process is complex involving various physical and chemical phenomena. The raw materials used can vary to a wide extent, from iron ore to dust recycling. The process takes place in a moving strand where a mixture of iron ore (sinter feed), fine coke, limestone and water is continuously charged to form a thick bed of approximately 40cm. Along the first meters of the strand the charge is ignited by burners. The hot gas, generated by the combustion of natural gas with air, is then sucked in through the packed bed from the wind boxes placed below the grate. The combustion of fines coke begins at the top of the layers, and as it moves, a relative narrow band of ignition zone moves down through the bed. Several chemical reactions and phase transformations take place within the bed, part of the materials melt when the local temperature reaches the melting temperature and as it moves, the solidification process occurs. The partial melting and diffusion within the materials causes the particle to agglomerate forming a continuous porous sinter cake. In general, the hot gas produced during sintering can also be re-circulated for better thermal efficiency. A schematic view of the sinter machine with recycling gas concept is presented in **Fig. 1**. The physicochemical and thermal phenomena involved are complex and numerous. Special mention is made to the phenomena of gas flow through the porous bed, gas-solid heat transfer, drying and several chemical reactions and phase transformations. Several attempts have been made aiming to predict the final properties of the sinter product. One of the most important parameter is the size distribution which influences strongly the sinter performance within the blast furnace.

Waters at al (Waters at al, 1989), developed a mathematical model to predict the final size distribution of the sinter, however, as they pointed out, the model did not considered the kinetics of the sintering phenomena, which strongly affect the final size distribution. Kasai et al (Kasai et al, 1991), investigated the influence of the sinter structure into the macroscopic sinter properties. A detailed explanation of the sintering mechanism and particles interaction were analyzed to clarify the bonding forces. They concluded that the void fraction and specific surface area are the main parameters influencing the cake strength. They also concluded that the significant driving forces of structural changes in the sinter cake are compressive and capillary ones. Akiyama et al(Akiyama et al,1992) investigated the heat transfer properties under the sinter bed conditions and established empirical correlations for the material conductivity. However, there are few comprehensive mathematical models describing the sintering process in an industrial machine such as the usual Dwight-Lloyd. Mitterlehner et al (Mitterlehner et al, 2004), presented a 1-D mathematical model of the sinter strand focusing on the progression speed of the sintering front. Nath et al, (Cumming, et al, 1990, Nath et al, 1997), developed a 2-D mathematical model based on transport equations, however, their analysis considered a few chemical reactions and the rate of phase transformations were simplified. A more detailed multi-phase model has been developed by Castro et al (Castro et al, 2005) which has been continuously updated. Therefore, a comprehensive mathematical model able to describe the chemical reactions coupled with momentum, energy and species transport has yet to be developed and applied to simulate the industrial scale of the sintering machine. In the present work, a 3-dimensional mathematical model of the sinter strand is developed based on the multiphase multi-component concept and detailed interactions between the gas and solid phases are addressed. Within the model framework are considered the following phenomena: a) dynamic interaction of the gas mixture with the solids; b) overall heat transfer of all phases; c) vaporization and condensation of water; d) decomposition of carbonates; e) reduction and oxidation of the iron bearing materials; f) fuel combustion and gasification; g) shrinkage of the packed bed; h) partial melt-solidification of the solids and i) phase changes. This model differs significantly of the former ones due to the concept of multiple and coupled phenomena treatment, three -dimensional treatment of the sinter strand and detailed mechanism of chemical reactions involved in the process. Therefore, this formulation represent a step forward on the task of constructing a comprehensive mathematical model of the iron ore sinter process capable of considering detailed phenomena which take place in the industrial operation. In this paper the actual sinter process is simulated and compared with industrial data. Afterwards the influence of the fuel quality is investigated and other alternative fuels such anthracite and biomasses are tested in order to indicate rational use of natural resources and develop cleaner industrial processes. Aiming to develop environmentally cleaner processes the dioxin and furans formation is investigated and optimum operation conditions are suggested.

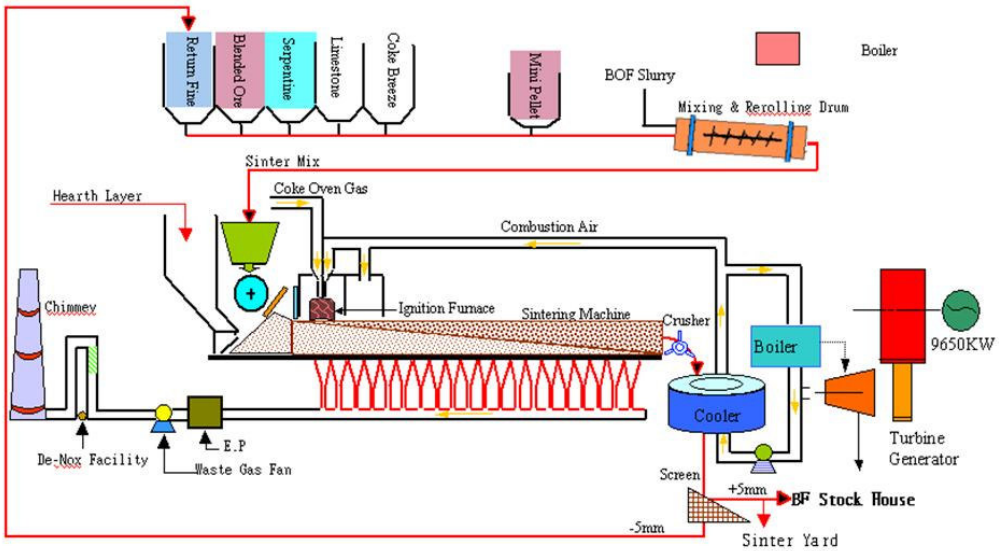

Figure 1 Lay out of the sintering process facilities

Figure 2 shows the inner phenomena of the sinter bed. Several chemical and phase transformation occurs in the sintering zone. The coke breeze or coal combust and form a so-called chemical front which is accompanied by a thermal front due to the endothermic reactions of combustion. A pre-heating and vaporization zone is developed due to the solid moisture and high temperature gas flowing from the combustion zone. Near the combustion zone, the iron ore in contact with the CO formed in the combustion zone reduces. Downstream, the gas is rich in O2 and re-oxidizes the solid and the solid is then cooled forming the sinter cake.

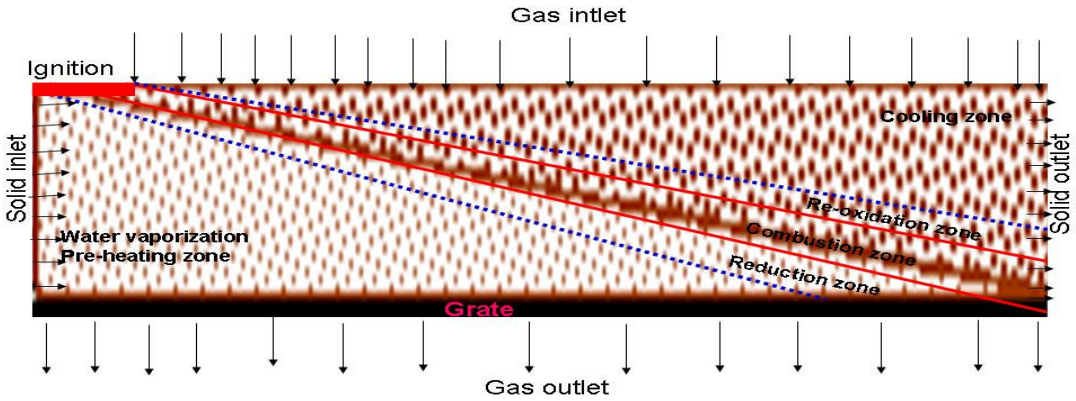

Figure 2 Inner characteristics of the sintering process of iron ore

2. Methodology

The model is three-dimensional and takes into consideration two distinct phases with momentum, energy and thermo physical properties defined by semi-empirical correlations. The momentum equations of the gas and solid phases takes into account the simultaneous interactions with one another. Within the solid phase the solid components are distinguished by their properties and the phase properties obeys the mixture rule. Figure 2 presents the two-phase model and the sintering mechanism. The sintering mechanism involve the formation of quasi-particles and the inner fuels particles combust furnishing heat to locally melt down of the iron ore and fluxing agent promoting the sintering reactions.

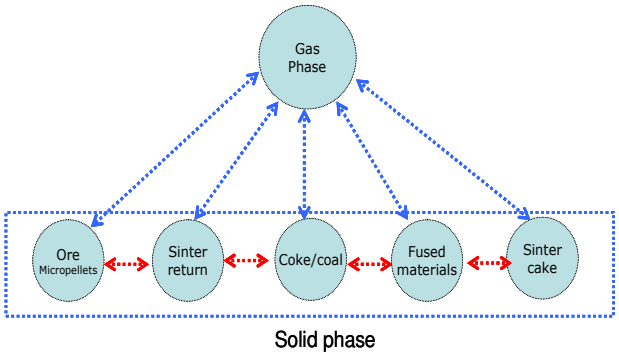

$$\sum_{k=ore}^{k=sin\,ter\,cake} f_k + \varepsilon_g = 1$$

Where f_m is the fractional volume of the solid components

a) Multi-phase concept

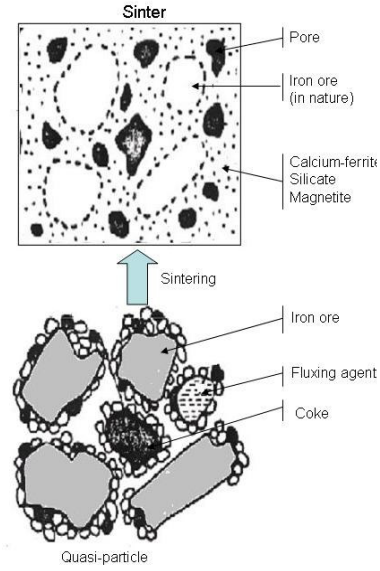

b) Sintering mechanism

Figure 3 The concept of multi-phase multi-component applied to the sintering phenomena – The basis for continuous model formulation of the sintering strand

2.1 General Conservation Equations

In order to accurately analyze the sintering process a three- dimensional model considering two phases interacting simultaneously interchanging momentum, energy and chemical species is proposed. The two phase model is described below as a set of strongly coupled conservation equations.

Gas phase:
Momentum equations:

$$\frac{\partial(\rho_g \varepsilon_g u_j)}{\partial t} + \mathrm{div}(\rho_g \varepsilon_g \vec{U}_g u_j) = \mathrm{div}[\varepsilon_g \mu_g \mathrm{grad}(u_j)] - \mathrm{grad}(P_g) + F_s^g - F_g^g \tag{1}$$

$$\frac{\partial(\rho_g \varepsilon_g)}{\partial t} + \mathrm{div}(\rho_g \varepsilon_g \vec{U}_g) = \sum_{i=1}^{nreacts} R_i^g \tag{2}$$

Energy equation:

$$\frac{\partial(\rho_g \varepsilon_g h_g)}{\partial t} + \mathrm{div}(\rho_g \varepsilon_g \vec{U}_g h_g) = \mathrm{div}\left[\varepsilon_g \frac{k_g}{C_{p,g}} \mathrm{grad}(h_g)\right] + E_s^g + \sum_{i=1}^{nreacts} R_i^g \Delta h_i \tag{3}$$

Chemical species equations:

$$\frac{\partial(\varepsilon_g \rho_g \phi_{g,k})}{\partial t} + \mathrm{div}(\varepsilon_g \rho_g \vec{U}_g \phi_{g,k}) = \mathrm{div}\left[\varepsilon_g \frac{D_k^g}{\varepsilon_g \rho_g} \mathrm{grad}(\phi_{g,k})\right] + \sum_{i=1}^{nreacts} R_i^g \beta_k \tag{4}$$

Where the indexes ***i*** and ***k*** indicate chemical reactions and chemical species, respectively. $\vec{U}$ is velocity field and u_j is velocity component on the directions (j=1,2,3). The subscripts ***g*** and ***s*** denote the gas and solid phases, respectively.

The solid phase can be expressed in a similar fashion as fallows:

Momentum:

$$\frac{\partial(\rho_s \varepsilon_s u_j)}{\partial t} + \mathrm{div}(\rho_s \varepsilon_s \vec{U}_s u_j) = \mathrm{div}[\varepsilon_s \mu_s \mathrm{grad}(u_j)] - \mathrm{grad}(P_s) - F_s^g - F_s^s \tag{5}$$

$$\frac{\partial(\rho_s \varepsilon_s)}{\partial t} + \mathrm{div}(\rho_s \varepsilon_s \vec{U}_s) = \sum_{i=1}^{nreacts} R_i^s \tag{6}$$

Energy equation:

$$\frac{\partial(\rho_s \varepsilon_s h_s)}{\partial t} + \mathrm{div}(\rho_s \varepsilon_s \vec{U}_s h_s) = \mathrm{div}\left[\varepsilon_s \frac{k_s}{C_{p,s}} \mathrm{grad}(h_s)\right] - E_s^g + \sum_{i=1}^{nreacts} R_i^s \Delta h_i \tag{7}$$

Chemical species equations:

$$\frac{\partial(\varepsilon_s \rho_s \phi_{s,k})}{\partial t} + \mathrm{div}(\varepsilon_s \rho_s \vec{U}_s \phi_{s,k}) = \mathrm{div}\left[\varepsilon_s \frac{D_k^s}{\varepsilon_s \rho_s} \mathrm{grad}(\phi_{s,k})\right] + \sum_{i=1}^{nreacts} R_i^s \beta_k \quad (8)$$

The phases and chemical species considered in this model are summarized in table 1. (Austin et al, 1997, Castro et al, 2001,2002, 2005)

Table 1 Equations used to model the sintering process

Equations of the gas phase			
Gas	Momentum	$u_{1,g}$, $u_{2,g}$, $u_{3,g}$, P_g, ε_g	
	Energy	h_g	
	Chemical Species	N_2, O_2, CO,CO_2, H_2O, H_2, SiO, SO_2, CH_4, C_2H_6, C_3H_8, C_4H_{10}	
Equations of the solid phase			
Solid	Momentum	$u_{1,s}$, $u_{2,s}$, $u_{3,s}$, P_s, ε_s	
	Energy	h_s	
	Chemical Species	Coke breeze	C,Volatiles, H_2O, Al_2O_3, SiO_2, MnO, MgO, CaO, FeS, P_2O_5, K_2O, Na_2O, S_2
		Iron ore	Fe_2O_3, Fe_3O_4, FeO, Fe, H_2O, Al_2O_3, SiO_2, MnO, MgO, CaO, FeS, P_2O_5, K_2O, Na_2O
		Return Sinter (bed)	Fe_2O_3, Fe_3O_4, FeO, Fe, H_2O, Al_2O_3, SiO_2, MnO, MgO, CaO, FeS, P_2O_5, K_2O, Na_2O
		Fused Materials	Fe_2O_3, Fe_3O_4, FeO, Fe, H_2O, Al_2O_3, SiO_2, MnO, MgO, CaO, FeS, P_2O_5, K_2O, Na_2O, CaO.Fe3O4, Al2O3.MgO
		Fluxing agent	CaO, H_2O, Al_2O_3, SiO_2, MnO, MgO, TiO_2
		Sinter cake	Fe_2O_3, Fe_3O_4, FeO, Fe, H_2O, Al_2O_3, SiO_2, MnO, MgO, CaO, FeS, P_2O_5, K_2O, Na_2O, CaO.Fe3O4, Al2O3.MgO

Total of 108 partial differential equations numerically solved using the finite volume technique.

2.2 Boundary conditions

The boundary conditions applied to the set of differential conservation equations of the model are of the inlet and outlet type for the gas phase at the top and the bottom faces, respectively. The energy equation uses as inlet boundary condition the average inflow temperature and at the outlet is assumed no temperature gradient. The inlet composition of the solid phase is specified together with solid temperature. For the velocity field, the gas is suctioned and the pressure gradient is used to specify the inlet flow rate at the top surface. The other boundaries are of symmetry type, where no flux is assumed, except for the temperature where a heat transfer coefficient is specified.

2.2 Source Terms

The interactions between the solid and gas phase is represented though the source terms of each equation. The source terms are due to external forces, interfaces interactions, chemical reactions and phase transformations. This section describes the models used for each of these phenomena.

2.3.1 Momentum sources

$$F_m = 150\mu_g \frac{1}{\left|\vec{U_g} - \vec{U_s}\right|}\left(\frac{\varepsilon_m}{(1-\varepsilon_m)\, d_m \varphi_m}\right)^2 + 1.75\rho_g \left(\frac{\varepsilon_m}{(1-\varepsilon_m)\, d_m \varphi_m}\right) \quad (9)$$

$$F_g^s = -F_s^g = \left[\sum_m f_m F_m\right] \left|\vec{U}_g - \vec{U}_s\right| \left(\vec{U}_g - \vec{U}_s\right) \quad (10)$$

Where ***m*** stands for the solid components (***m***=ore, sinter, fluxing etc).

2.3.2 Heat transfer

The inter-phase heat transfer considers a local effective coefficient which takes into considerations the combined effect of convection and radiation within the packed bed[Akiyama].

$$\dot{E}_g^s = -\dot{E}_s^g = h_{g-s} A_{s-g} \left[T_s - T_g \right] \tag{11}$$

$$h_{s-g} = \frac{k_g}{d_s} \left[2.0 + 0.39 \left(Re_{g-s} \right)^{0.5} \left(Pr_g \right)^{1/3} \right] \tag{12}$$

The granular specific surface area is modeled as in eq. 13.

$$A_{s-g} = \sum_m \left(f_m \frac{6\varepsilon_m}{d_m \varphi_m} \right) \tag{13}$$

The variables and symbol with their respective units are summarized in table 2

Table 2 Variables used in the model

A_{s-g}	Specific area of the bed [m^2/m^3]		**Subscript**
$\dot{E}_g^s$	Rate of energy exchanged between gas and solid phases (kW)	g	Gas phase
f_m	Volume fraction of solid components (-)	s	Solid phase
F_g^s	Momentum transfer from gas phase to solid phase (N/m^3)	i	Index for chemical reactions
h_{g-s}	Overall heat transfer coefficient between gas and solid (W/m^2 K)	j	Index for phase velocity components
k_g	Thermal conductivity of gas phase (W/mK)	k	Index for phase mass fraction
Pr_g	Prandtl number relating to the gas phase	m	Index to account for phase component

2.3.3 Chemical Reactions

Table 2 Chemical reactions considered in the model

R_i	Chemical Reactions
Reduction by CO	
1_i	$\mathbf{3\,Fe_2O_3}(i) + \mathbf{CO}(g) \rightarrow 2\mathbf{Fe_3O_4}(i) + \mathbf{CO_2}(g)$ $(i \rightarrow ore, sinter, fines, etc)$
2_i	$\frac{\mathbf{w}}{\mathbf{4w-3}}\mathbf{Fe_3O_4}(i) + \mathbf{CO}(g) \rightarrow \frac{3}{4w-3}\mathbf{Fe_wO}(i) + \mathbf{CO_2}(g)$ $(i \rightarrow ore, sinter, fines, etc)$
3_i	$\mathbf{Fe_wO}(i) + \mathbf{CO}(g) \rightarrow w\,\mathbf{Fe}(i) + \mathbf{CO_2}(g)$ $(i \rightarrow ore, sinter, fines, etc)$
Reduction by H_2	
4_i	$\mathbf{3\,Fe_2O_3}(i) + \mathbf{H_2}(g) \rightarrow 2\mathbf{Fe_3O_4}(i) + \mathbf{H_2O}(g)$
5_i	$\frac{\mathbf{w}}{\mathbf{4w-3}}\mathbf{Fe_3O_4}(i) + \mathbf{H_2}(g) \rightarrow \frac{3}{4w-3}\mathbf{Fe_wO}(i) + \mathbf{H_2O}(g)$
6_i	$\mathbf{Fe_wO}(i) + \mathbf{H_2}(g) \rightarrow w\,\mathbf{Fe}(i) + \mathbf{H_2O}(g)$ $(i \rightarrow ore, sinter, fines, etc)$
Re-oxidation of solids	
7_i	$\mathbf{w\,Fe}\ (i) + \frac{1}{2}\mathbf{O_2}(g) \rightarrow \mathbf{Fe_wO}(i)$
8_i	$\frac{3}{4w-3}\mathbf{Fe_wO}(i) + \frac{1}{2}\mathbf{O_2}(g) \rightarrow \frac{\mathbf{w}}{\mathbf{4w-3}}\mathbf{Fe_3O_4}(i)$
9_i	$\mathbf{2\,Fe_3O_4}(i) + \mathbf{O_2}(g) \rightarrow 3\mathbf{Fe_2O_3}(i)$ $(i \rightarrow ore, sinter, fines, etc)$
Gasification of carbon	

10_i	$C(i)+\frac{1}{2}\mathbf{O_2}(g)\rightarrow CO(g)$
11_i	$C(i)+\mathbf{O_2}(g)\rightarrow CO_2(g)$
12_i	$C(i)+\mathbf{CO_2}(g)\rightarrow 2CO(g)$
13_i	$C(i)+\mathbf{H_2}O(g)\rightarrow H_2(g)+CO(g)$ $(i\rightarrow \text{coke breeze or coal})$
Gasification of volatiles	
14_i	$\text{Volatiles}(i)+\alpha_1O_2(g)\rightarrow \alpha_2CO_2(g)+\alpha_3H_2O(g)+\alpha_4N_2(g)$
15_i	$\text{Volatiles}(i)+\alpha_5CO_2(g)\rightarrow \alpha_6CO(g)+\alpha_7H_2(g)+\alpha_8N_2(g)$ $(i\rightarrow \text{coke breeze or coal})$
Water gas shift	
16	$CO_2(g)+H_2(g)\rightarrow CO(g)+H_2O(g)$
Phase transformation	
17_i	$H_2O(i)\leftrightarrow H_2O(g)$ $(i\rightarrow \text{ore, sin ter, coke})$
18_i	$CaO(i)\leftrightarrow CaO(l)$
19_i	$MgO(i)\leftrightarrow MgO(l)$
20_i	$MnO(i)\leftrightarrow MnO(l)$
21_i	$Al_2O_3(i)\leftrightarrow Al_2O_3(l)$ $(i\rightarrow \text{ore, sin ter, coke})$
22_i	$CaO(i)+FeO(i)\leftrightarrow (CaO).(FeO)$ $(i\rightarrow \text{ore, sin ter, coke})$
23_i	$2CaO(i)+FeO(i)\leftrightarrow (CaO)_2.(FeO)$ $(i\rightarrow \text{ore, sin ter, coke})$

3. Results and Discussions

3.1 Analysis of the Actual Sinter Plant Operation Technique

The actual sinter machine operation requires a typical temperature distribution in order to drive the sintering reactions. As can be observed in figure 4, the combustion front develops a narrow high temperature region due to the combustion of carbon releasing energy for both solid and gas phases.

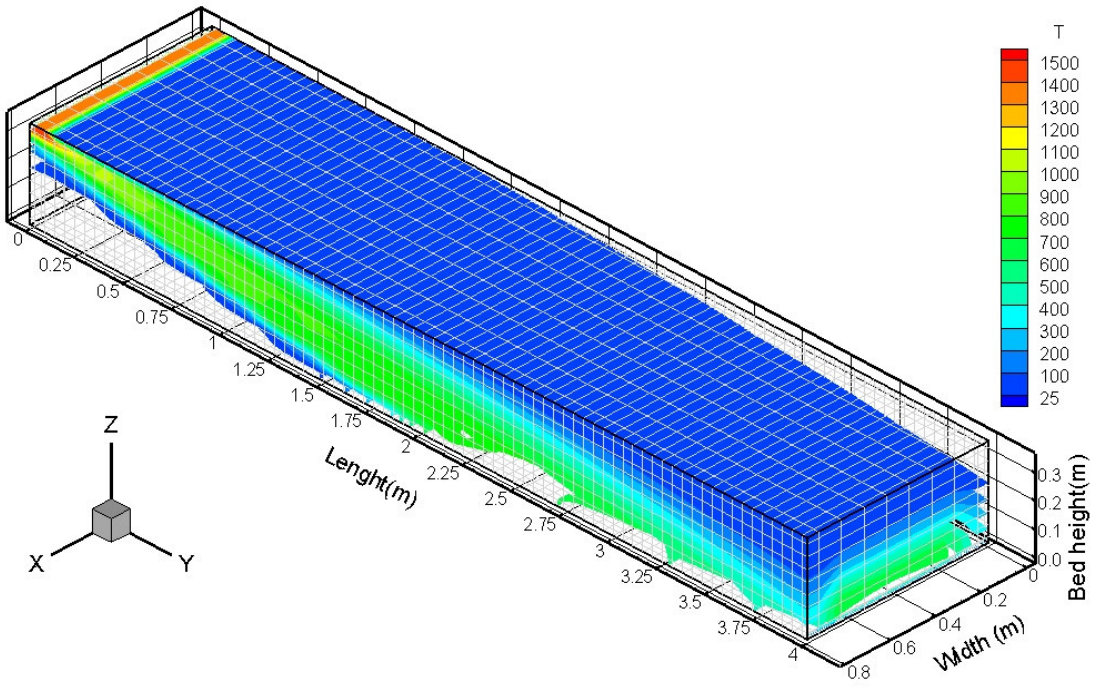

Figure 4 Gas temperature distribution within the sinter bed

In figure 5 the combustion front is evidenced. In order to obtain the sintering properties of strength and reducibility, the major blast furnace requirements, is desirable narrow combustion front with a temperature peak around 1350 ^oC, depending of the sinter basicity and iron ore genesis. In actual sinter

operation practice a residence time around 2 min is suitable for high sinter properties, which correspond to a combustion front thickness of about 40 cm, as shown in fig. 5.

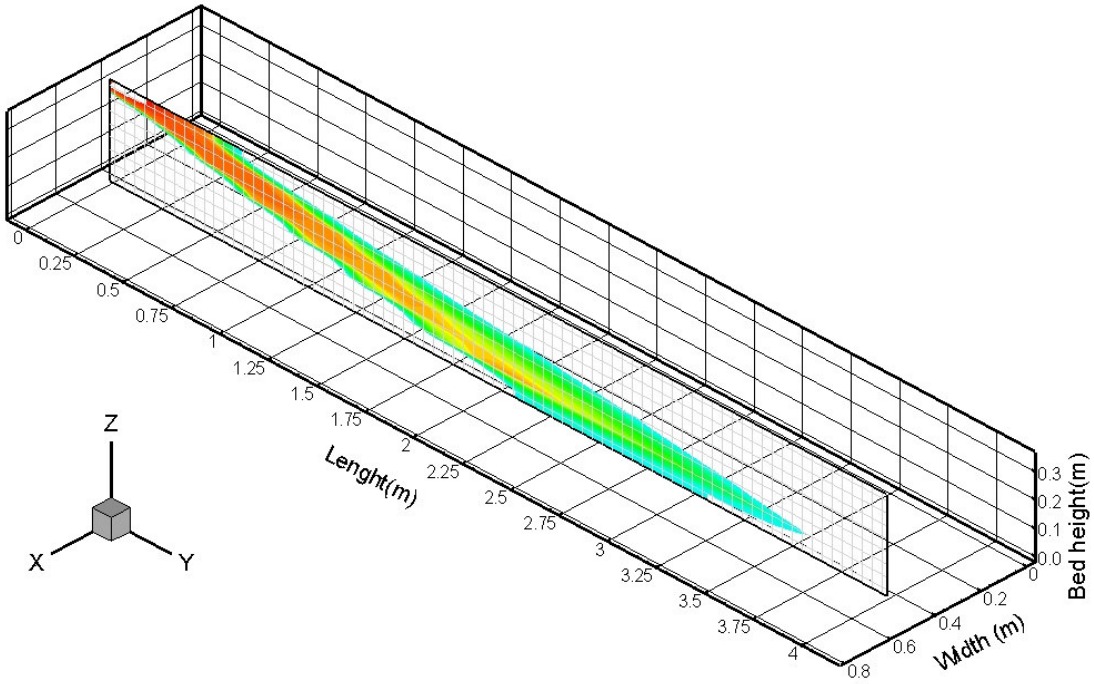

Figure 5 the sinter front at a central vertical plane. Colors levels corresponding to temperatures as in figure 4.

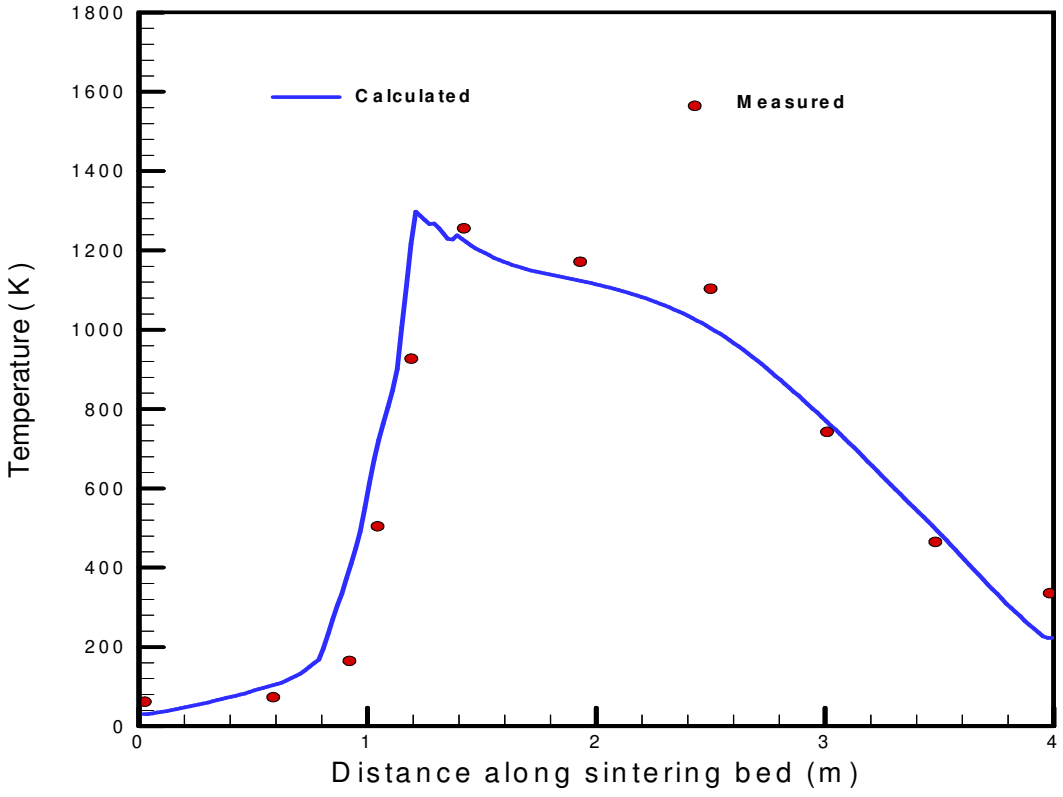

Figure 6 Comparison of measured and calculated temperature along the sinter strand at the industrial plant (5 cm)

Figure 6 and 7 shows comparison of measured and calculated temperature along the sintering strand. The measured values were obtained by placing thermocouples within the sinter layer and recorded. The calculated values are the average temperature of gas and solid phases. A quite good agreement of model predictions and measurements were obtained for both locations (fig 6 – 5 cm depth from top to bottom and fig 7 5 cm from bottom to top)

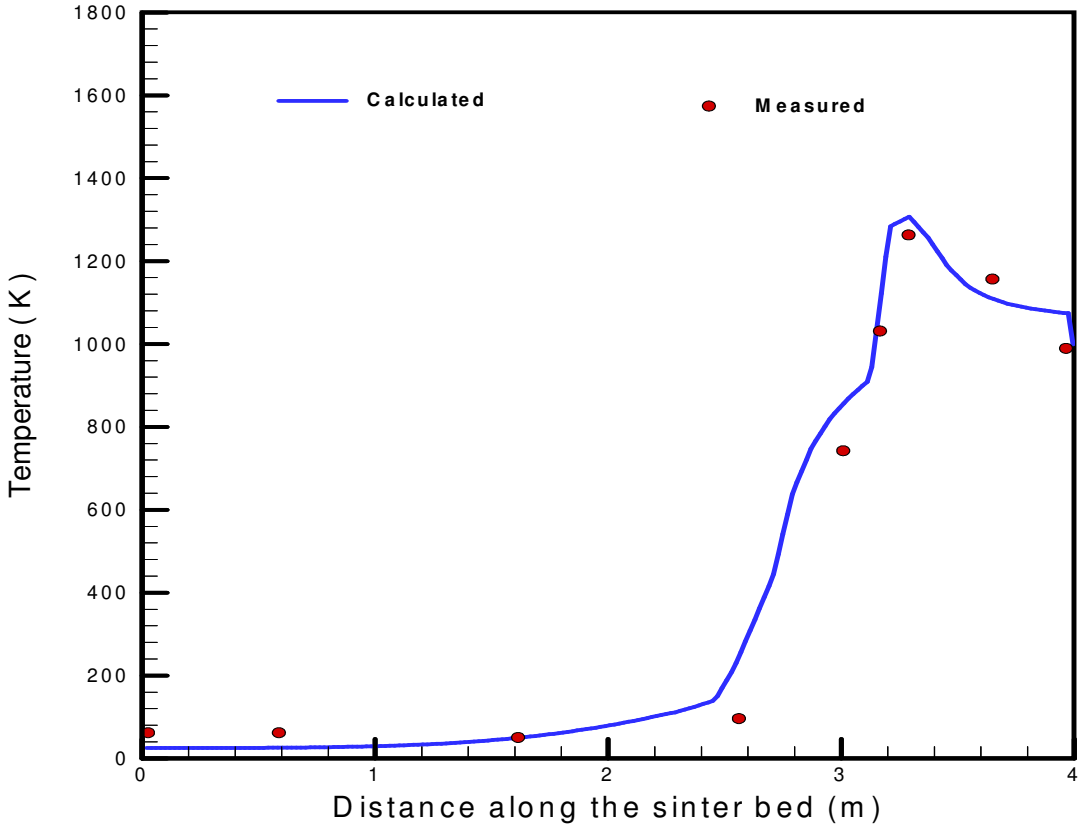

Figure 7 Comparison of measured and calculated temperature just above the grate at the industrial plant

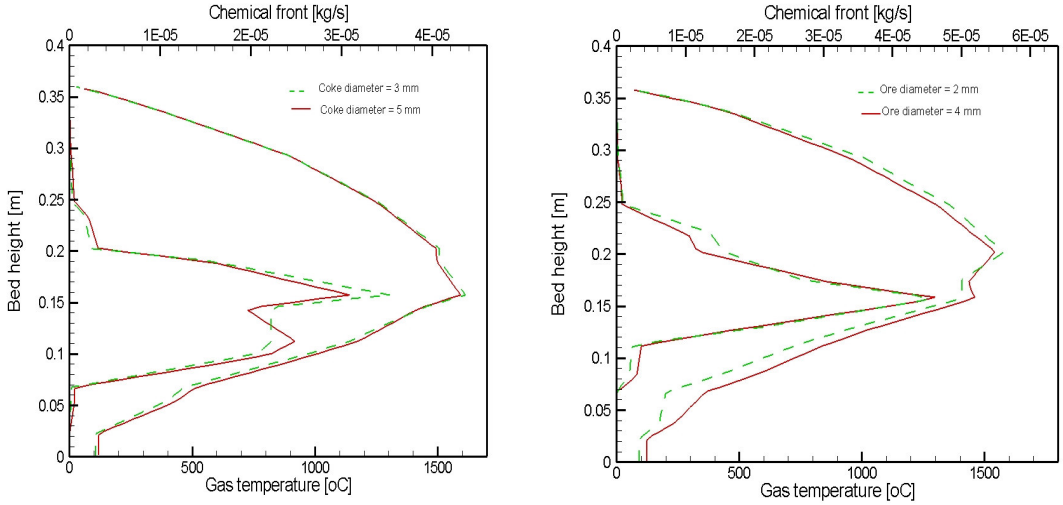

a) Effect of mean diameter of coke breeze

b) Effect of mean diameter of iron ore

Figure 8 Investigation of the effect of raw materials physical properties on the sintering phenomena

The coke breeze and iron ore bearing materials charged are technological parameters of great interest due to their effect on the fluid dynamics and reaction rates. Figure 8 shows the effect of particle size on the location and thickness of the combustion zone. As iron ore diameter increases the gas and solid decrease the heat exchange and the maximum temperature decreased about 40 ^{o}C. On the other hand decreasing the coke breeze mean diameter the reaction rates enhanced and the region of higher temperature increased.

3.2 Application for Advanced Operations

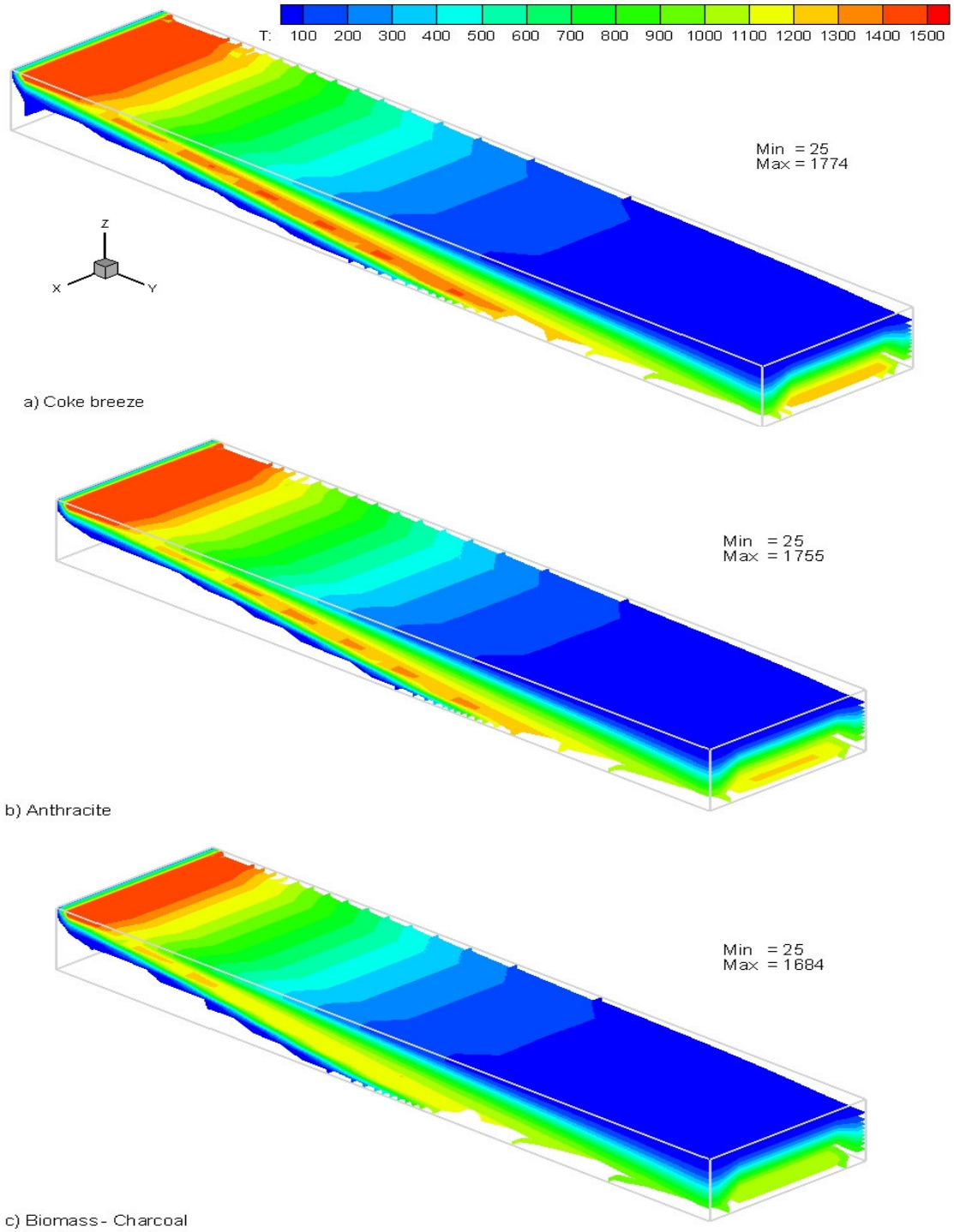

Figure 9 Investigation of alternatives fuels

The fuels used in the metallurgical processes are of increasing concern due to the direct use of natural resources as mineral coals oil and natural gas. Figure 9 shows the effect of a hypothetical replace of coke

breeze by anthracite and biomasses with potential reductions of cost and environmental load. These alternatives have shown attractive features, however the temperature peak is lower and the speed of the strand has to be reduced which leads to reduction on the productivity. However as environmental pressure has increased, these alternatives will become economically viable in near future.

4. Conclusions

A multi-phase mathematical model has been developed and applied to simulate the sinter plant of an integrated steel industry. The model is based on transport equations of momentum energy and chemical species coupled with chemical reaction of reduction, combustion, oxidation and physical transformation such as melting water evaporation and condensation. The computational code was implemented in Fortran 90/95 and the finite volume method based on the SIMPLE algorithm with staggered velocity projections. The model results were confronted with industrial measurements and showed good agreement. The model was used to investigate unusual operation techniques such as higher fuel size and different fuels aiming to increase the possibility of blending raw materials for using in the sintering process.

5. Acknowledgements

The authors thanks to CNPq and CAPES for financial support

6. Referências

Akiyama, T. Ohta, H. Takahashi, R. Waseda, O. and Yagi, J. , 1992 “Measurementand Oxide and Porous Modeling of lron Ore Thermal Conductivity for Dense iron Agglomerates in Stepwise Reduction” ISIJ Int., Vol. 32, pp. 829-837.

Austin, P.R., Nogami, H. and Yagi, J., 1997, “A Mathematical Model of Four Phase Motion and Heat Transfer in the Blast Furnace”. ISIJ Int., Vol. **37**, pp. 458-467.

Austin, P.R., Nogami, H. and Yagi, J., 1997, “A Mathematical Model for Blast Furnace Reaction Analysis Based on the Four Fluid Model”. ISIJ Int., Vol. **37**, pp. 748-755.

Castro, J.A. Silva, A.J. , Nogami, H. e Yagi, J. , 2005 “ Tecnologia em Metalurgia e Materiais, Vol 2, pp 45-52.

Castro, J.A, 2001, “A multi-dimensional transient mathematical model of the blast furnace based on the multi-fluid model”. Ph.D thesis, IMRAM – Institute for multidisciplinary research for advanced materials – Tohoku University – Japan

Castro, J.A., Nogami, H. and Yagi, J., 2002, “Three-dimensional Multiphase Mathematical Modeling of the Blast Furnace Based on the Multifluid Model”. ISIJ Int., Vol. 42, pp. 44-52.

Cumming, M.J. and Thurlby, J. A. , 1990 “ Development in Modelling and Simulation of Iron Ore Sintering”, Ironmaking and Steelmaking, vol 17, pp 245-254.

Kasai, E. Batcaihan, B. Omori, Y. Sakamota, N. and Kumasaka, A.,1991 “Permeation Characteristics and Void Structure of lron Ore Sinter Cake” ISIJ Int., Vol. 31, pp. 1286-1291.

Mitterlehner, J. Loeffler, G. Winter, F., Hofbauer, H., Schmid, H. Zwittag, E. , Buergler, H. Pammer, O. and Stiansy, H. , 2004 “Modeling and Simulation of Heat Front Propagation in the Iron Ore Sintering Process”, ISIJ Int., Vol. 44, pp. 11-20.

Nath, N. K. Silva, A.J. and Chakraborti, N. , 1997 “Dynamic Process Modelling of Iron Ore Sintering”, Steel Research, vol 68, pp 285-292.

Waters, A. G. Litster, J.D. and Nicol, S.K. , 1989 “AMathematical Model for the Multicomponent Sinter Feed” ISIJ Int., Vol. 29, pp. 274-283.